Anderson Hamiltonian description of the experimental electronic structure and magnetic interactions of copper oxide superconductors

Zhi-xun Shen
Stanford Electronics Laboratory, Stanford University, Stanford, California 94305
and Department of Applied Physics, Stanford University, Stanford, California 94305

J. W. Allen*
Xerox Palo Alto Research Center, 3333 Coyote Hill Road, Palo Alto, California 94304

J. J. Yeh
Stanford Electronics Laboratory, Stanford University, Stanford, California 94305

J.-S. Kang*
Xerox Palo Alto Research Center, 3333 Coyote Hill Road, Palo Alto, California 94304
and Department of Physics and Institute for Pure and Applied Physical Sciences, University of California at San Diego, La Jolla, California 92093

W. Ellis
Los Alamos National Laboratory, Los Alamos, New Mexico 87545

W. Spicer and I. Lindau
Stanford Electronics Laboratory, Stanford University, Stanford, California 94305

M. B. Maple, Y. D. Dalichaouch, and M. S. Torikachvili
Department of Physics and Institute for Pure and Applied Physical Sciences, University of California at San Diego, La Jolla, California 92093

J. Z. Sun and T. H. Geballe
Department of Applied Physics, Stanford University, Stanford, California 94305
(Received 20 July 1987)

We describe valence-band and core-level photoemission data for copper oxide superconductors using the Anderson Hamiltonian applied to an impurity-cluster configuration-interaction model. We obtain experimental values of the parameters of the model, the copper$\rightleftarrows$oxygen charge-transfer energy $\Delta\sim 0.4$ eV, the d-d Coulomb interaction $U\sim 6$ eV, and the ligand-d hybridization $T\sim 2.4$ eV. Using these parameters, we evaluate the linear Cu—O—Cu superexchange interaction J and find it is dominated by the charge-transfer fluctuations. The magnitude obtained for J is much larger than typical Néel temperatures of these materials, and is somewhat larger than that estimated from applying the resonating-valence-bond picture to La_2CuO_4. We point out that for $\Delta \ll U$ and $T \gg \Delta$ the charge-transfer degrees of freedom, and the lattice aspects of the Anderson lattice Hamiltonian, should not be neglected in constructing models for the high-T_c superconductivity. We also emphasize our resonant-photoemission result that the very small density of states at or near the Fermi level in all these materials has a substantial contribution from Cu $3d$ states, suggesting their importance for the superconductivity. We report other details of the resonant-photoemission data involving La and Ba states in the materials containing these elements.

I. INTRODUCTION

An understanding of the origin of the large superconducting transition temperatures T_c of the superconducting copper oxides[1-11] will require an understanding of their electronic structure. In the past seven years it has been established[12-22] that experimental electron spectra of various insulating transition-metal compounds are best described using the Anderson Hamiltonian. This Hamiltonian models the energetics of two charge fluctuation processes: the polar type, $d_i^n d_j^n \rightleftarrows d_i^{n-1} d_j^{n+1}$ (where i and j label transition metal sites and n is the number of d electrons), involving the d-d Coulomb energy U, and the charge-transfer type, $d_i^n \rightleftarrows d_i^{n+1}L$ (where L denotes a hole in the anion valence band), involving the energy Δ, related to the electronegativity of the anion and the Madelung potential. Charge-transfer fluctuations are directly enabled by hybridization (matrix element T) between the transition-metal d states and the anion valence-band states, and polar fluctuations result from higher-order hy-

 ©1987 The American Physical Society

bridization processes. When U is large compared to the one-electron bandwidth, it is expected that one-electron density-functional theory will not provide a good description of the electronic structure, apart from the ground-state energy and charge density. In addition, when $\Delta < U$, it is expected that the charge-transfer fluctuations will dominate the low-energy physics, so that a simple Mott-Hubbard description containing only U will not suffice, unless it is possible to regard Δ as a kind of hybridization-screened effective U, as we discuss further below. Recently the impurity Anderson Hamiltonian has been applied[18] to describe the band gaps of transition-metal compounds and to provide a phase diagram based on Δ and U for classifying various compounds.

Various mechanisms[23-32] have been proposed to account for the high value of T_c, based on different models of the underlying electronic structure. Some of these models use the density-functional band calculation to discuss the electron-phonon interaction and phonon-mediated superconductivity in a more or less conventional way. Others[23-25,29,32] employ a Hubbard Hamiltonian for the Cu $3d$ electrons, and emphasize electron-electron correlation effects. For example, the resonating-valence-bond picture[23-25] introduces a nonconventional pairing mechanism derived from the antiferromagnetic exchange interaction J between Cu $3d$ electrons on different sites. Other[27,28,30,31] nonconventional mechanisms proceed from the Anderson lattice model, which is an extended Hubbard model including both the Cu $3d$ and the oxygen $2p$ electrons, as described above.

To guide theory in the choice of a model, it is important to determine at least roughly the magnitudes of the model parameters. As we report below, and as found by others,[33-37] there are large differences between measured valence-band photoelectron spectra and the density-functional eigenvalue spectrum, which imply a large value for U. In particular, there is a valence-band feature at about 12.4 eV below the Fermi level. Such a satellite feature is observed in copper dihalides[12,13] and copper oxides,[38,39] where it has been assigned to $3d^8$ final states. For the dihalides the valence-band spectra and the copper $2p$ core-level spectra, which also show satellites, have been analyzed[12-14] to extract values for the parameters Δ, T, and U using a cluster-impurity approximation to the Anderson Hamiltonian, as described further below. Although such a satellite feature is not apparent in their valence-band x-ray photoemission spectroscopy (XPS) spectra of the superconducting copper oxides, Fujimori *et al.*[33] have plausibly assumed that it occurs and have made a similar analysis for these materials.

In Secs. II–V we present soft x-ray resonant photoemission spectra of the valence band and XPS spectra of the copper $2p$, and various other core levels of $YBa_2Cu_3O_{7-\delta}$, La_2CuO_4, and $La_{1.8}Sr_{0.2}CuO_4$. The data for all our samples clearly show the existence of the high-energy valence-band feature, the energy of which is actually 1 eV larger than assumed by Fujimori *et al.*[33] In Sec. VI we describe sample and time dependences of the spectra and discuss other caveats. In Sec. VII we give a detailed analysis of all the data using the cluster approximation to the Anderson Hamiltonian and extract values for the model parameters $U \sim 6$ eV, $\Delta \sim 0.4$ eV, and $T \sim 2.4$ eV. In Sec. VIII we explore the consequences of the model further and evaluate the antiferromagnetic superexchange coupling J between Cu sites. Estimates of J in these materials based on spectroscopic parameters have not been given before. For the range of parameters found, the usual perturbative superexchange expressions are not adequate because Δ is small, which leads to values of J that are the order of magnitude of, but somewhat larger than, that[24,25] estimated from applications of the resonating valence bond model. In Sec. IX we give some concluding discussion of the implications of the parameter values in terms of the generalized phase diagram of Ref. 18. We note that during the course of our work, other workers[33-37,40-42] have independently obtained some of the experimental results we report.

Our results lead to the conclusion that the electronic structures of the high-T_c materials are not well given by the single-particle band picture, and that in addition to high-energy polar fluctuations at energy U, microscopic models should also include lower-energy charge-transfer fluctuations at energy Δ. In the cluster model used here, the least binding energy-occupied states involve Cu valence fluctuations between $3d^9$ and $3d^{10}$ and correlated occupations of the Cu $3d$ and oxygen $2p$ states, consistent with our experimental finding that there is a substantial Cu $3d$ component in the states near and at the Fermi energy. We note that superconductivity models that utilize the charge-transfer degrees of freedom in one way or another have been proposed[27,28,30,31] and that optical data have been interpreted[43] as showing a charge-transfer gap of ~ 0.5 eV.

II. EXPERIMENT

Samples of the superconducting copper oxides were prepared at the University of California at San Diego (UCSD) and Stanford. The UCSD La_2CuO_4 and $La_{1.8}Sr_{0.2}CuO_4$ compounds were prepared by means of a coprecipitation technique followed by pressing and sintering, while the UCSD $YBa_2Cu_3O_{7-\delta}$ compound was fabricated by mixing the Y and Cu oxides, and Ba carbonate followed by pressing and sintering twice, as described in Ref. 11. The Stanford samples of La_2CuO_4 and $La_{1.8}Sr_{0.2}CuO_4$ were prepared by mixing the appropriate amounts of La, Sr, and Cu oxides, pressing and sintering twice, and then oven cooling. A sample of $YBa_2Cu_3O_{7-\delta}$ from the Stanford Research Institute (SRI) was made by a coprecipitation technique. The samples made by coprecipitation generally seem denser, as indicated by their mechanical properties under the cleaning techniques described below, and by their higher photoemission count rates. Most of the samples measured were determined to be single phase by x-ray diffraction. Superconductivity was verified by measurement of the resistivity and susceptibility, which showed sharp transitions with values of T_c similar to those reported elsewhere.[1-11]

Room-temperature resonant photoemission measurements were performed at the Stanford Synchrotron Radiation Laboratory (SSRL) using photons obtained from

the grasshopper monochromator on beam line III-1. A commercial double-pass cylindrical mirror analyzer (CMA) was used to analyze the kinetic energies of the emitted electrons, and clean surfaces were obtained both by fracturing and by scraping with a diamond file *in situ* in a vacuum chamber having a base pressure of 7×10^{-11} Torr. Samples for scraping were mounted in the chamber before the experiment and therefore were exposed to the elevated temperatures ($\sim$180 °C) of the chamber bake, while samples for fracturing were transferred into the chamber via a fast-entry lock during the course of the experiment. The Stanford and SRI samples were mounted for scraping and the UCSD samples were mounted for fracturing, except in the case of the UCSD $YBa_2Cu_3O_{7-\delta}$, which was divided so that samples for both fracturing and scraping could be prepared. Identical spectra were obtained from this sample using each preparation method, except that the fractured surface gave higher intensity, presumably because it was smoothed. This provides evidence that the different mechanical cleaning methods do not alter the spectra, and that the different thermal histories are also not important. The resolution of the data is 0.45 eV, unless otherwise indicated, determined mostly by the CMA. The Fermi level of the system was determined from the valence-band spectrum of a gold sample evaporated onto a stainless-steel substrate *in situ*. The beam flux was measured from the yield of a stainless-steel mesh, and the spectra reported below have all been normalized to this yield.

X-ray photoemission spectra of the Cu $2p$ core levels of Cu, CuO, and La_2CuO_4 were obtained at Stanford using a system essentially like that used at SSRL, and of La_2CuO_4, $La_{1.8}Sr_{0.2}CuO_4$, and $YBa_2Cu_3O_{7-\delta}$ at the Xerox Palo Alto Research Center (Xerox PARC) using a Vacuum Generators ESCALAB. The resolution for these measurements was $\sim$1.3 eV. The first two of the samples measured at Xerox PARC were the same ones used for resonant photoemission. The Cu sample was prepared by evaporation *in situ* onto a stainless-steel substrate and the CuO sample was prepared from commercial material of 99.999% purity supplied in a sealed bottle. The CuO was kept sealed until just before use, when it was pressed and then fastened to a substrate with silver epoxy. For the XPS measurements at Stanford and Xerox, respectively, the Fermi level was calibrated from the valence band and core levels of an evaporated gold sample or a solid silver sample cleaned by sputtering. Pressures in the chambers for the XPS measurements were between 1×10^{-10} and 5×10^{-10} Torr, determined mostly by sample outgassing. The samples were at room temperature for the measurements, except for $La_{1.8}Sr_{0.2}CuO_4$, which was also measured at 110 K and gave the same spectra at both temperatures.

Several unsuccessful attempts to measure the x-ray inverse photoemission, i.e., bremsstrahlung isochromat spectra (BIS) of these samples, were made. Either the spectra were badly distorted by charging, or it was found from the Cu $2p$ XPS spectra measured before and after the BIS experiment that the electron beam had changed the Cu configuration from a mix of d^9 and d^{10} to purely d^{10}. This experience shows that BIS experiments in which the sample is not characterized before and after by XPS core-level spectra are not conclusive.

III. VALENCE-BAND SPECTRA AND COMPARISON WITH BAND CALCULATIONS

The valence-band spectra displayed some time and sample dependences. This section and the next describe data taken in the time interval after surface preparation in which no changes occurred. The time dependences observed and various other caveats are described in Sec. V, and the sample dependences are pointed out as appropriate. All the spectra show a peak in the vicinity of 9 eV. It appears that this peak has both an intrinsic component and a carbon-induced component. Evidence for the latter is as follows. This peak decreases dramatically when the sample is cleaned, and for the clean surfaces varies in height from sample to sample in a way which correlates with the magnitude of the carbon $1s$ peak observed in the XPS measurements described in Sec. V. The energy of the peak is typical for the $2p$ emission of carbon contamination, as is its photon energy dependence, and so the peak is assigned to grain boundary carbon. The peak is smallest for samples prepared without carbonates. Evidence for the intrinsic component is that new samples, measured subsequently to our performing the other experiments reported in this paper, display the 9-eV valence-band peak but no carbon $1s$ peak. It seems likely that the intrinsic contribution involves oxygen states which have energies and photoemission properties generally similar to carbon states.

Figure 1 shows the energy distribution curves (EDC's) of different samples at a photon energy of 75 eV. The $YBa_2Cu_3O_{7-\delta}$ curves have been corrected for effects due to second-order light as described in the next section. Also shown are theoretical EDC's obtained by addition of partial densities of state from band calculations,[44,45] weighted by appropriate photoemission cross sections. At a photon energy of 75 eV the atomic cross section[46] of Cu $3d$ is about 4.5 times larger than that of O $2p$, not including the Cu resonance effects described further below. At 75 eV the Y $4d$ cross section[46] has reached its Cooper minimum and hence is 1 to 2 orders of magnitude smaller than for Cu or O. The Ba $5d$ cross section is also an order of magnitude smaller than for Cu or O at this photon energy. A straightline inelastic background has been added to the theoretical curves to facilitate comparison with the data. It is apparent that there is not good agreement between any of the experimental and theoretical curves.

Spectra from two $YBa_2Cu_3O_{7-\delta}$ samples are shown in Fig. 1. The main bands of the two samples differ in that No. 2 has a shoulder at -2.5 eV which is essentially absent for No. 1. This shoulder disappears as the sample ages. From its time and photon energy dependences, it may be due to Y_2O_3, as discussed further in Secs. V and VI. For $YBa_2Cu_3O_7$, the band calculation predicts that the valence band should have two features with maxima at -0.8 and -3.8 eV, and extend only 5.5 eV below the Fermi level. However, in both the experimental EDC's the valence band extends to -7 eV and the center of

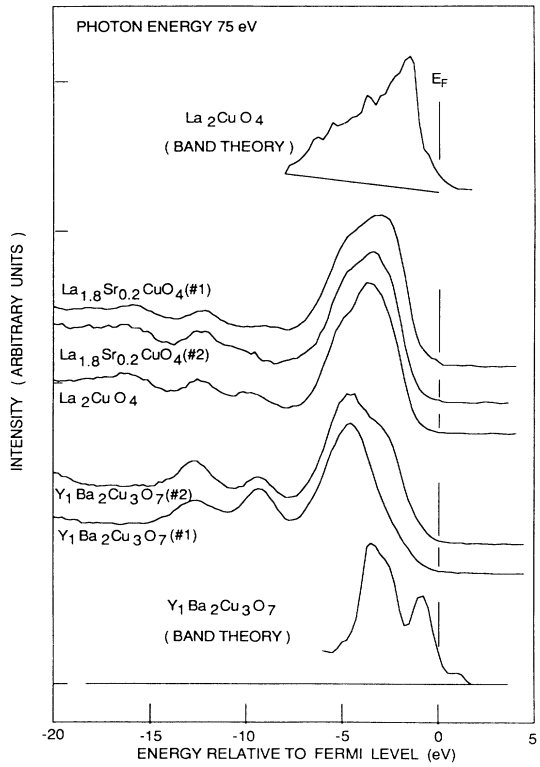

FIG. 1. Comparison of the experimental, room-temperature valence-band spectra with band theoretical spectra. The various sample origins are $La_{1.8}Sr_{0.2}CuO_4$, No. 1 (UCSD), No. 2 (Stanford); La_2CuO_4 (Stanford); $Y_1Ba_2Cu_3O_{7-\delta}$, No. 1 (UCSD), No. 2 (SRI). The photon energy used maximizes the Cu d^8 satellite at -12.5 eV. Effects due to second-order light have been removed from the $YBa_2Cu_3O_{7-\delta}$ spectra as described in the text.

gravity is shifted to higher binding energy than in the theory. The density of states at the Fermi level, E_F, is so small that the Fermi edge is not clearly observed in contrast with the predicted value of 25% of the value of the maximum of the valence band.

For $La_{1.8}Sr_{0.2}CuO_4$ the data from two different samples are essentially identical except for the magnitudes of the peaks with a carbon contribution. The theoretical curve for La_2CuO_4 differs much more from that for $YBa_2Cu_3O_{7-\delta}$ than do the experimental curves of all three materials. Considering the experimental curves for La_2CuO_4 and $La_{1.8}Sr_{0.2}CuO_4$ together, the experimental maximum occurs at -2.8 eV compared to the theoretical value of -1.5 eV, and the experimental density of states at E_F is again much lower than the theoretical value of 15% of the value of the valence-band peak. Only for sample No. 2 of $La_{1.8}Sr_{0.2}CuO_4$, for which there was a particularly high count rate, could the Fermi edge be observed, as shown in the inset of Fig. 2.

To summarize, for the main bands of all the samples (a) the experimental peaks or centroids are shifted to higher energy than in the theory, (b) the shapes and widths of the spectra from theory and experiment are quite different, and (c) the experimental density of states at E_F is much smaller than in the theory. These discrepancies are particularly significant for the states near E_F, since these are the states important for superconductivity in conventional theories.

Another difference of great significance between band theory and experiment is the presence of the feature at -12.5 eV in each of the spectra of Fig. 1. As explained in Sec. IV, this feature can be identified as having a Cu $3d$ origin by the fact that it is largest for the photon energy about 75 eV, just above the Cu $3p$ absorption edge. Such high binding-energy "satellite" features, not predicted by band theories, but often observed in the transition metals and compounds, signal the presence of a large $3d$ Coulomb correlation energy U.[12,47,48] The simplest description of this feature is obtained using the cluster model of Sec. VII, in which it corresponds to Cu d^8 final states pushed out of the valence band by U. That the $3d^8$ states occur at such a high energy means that charge fluctuations to $3d^8$ must be strongly suppressed in the ground state, and that Cu^{3+} states are essentially impossible, even in compounds where the formal Cu valence state is Cu^{3+}, such as $NaCuO_2$.[49]

IV. RESONANCE PHOTOEMISSION FROM Cu, La, Ba, AND OTHER PHOTON ENERGY DEPENDENCES

The photon energy ($h\nu$) dependences of the valence-band emissions associated with Cu, La, and Ba display resonance effects that can aid in their identification. For Cu the resonance occurs near the $3p$ absorption edge, $h\nu \sim 70$ eV, and for La and Ba, it occurs near the $4d$ absorption edges, $h\nu \sim 100$ eV. It is generally understood[48,50] that this resonant photoemission spectroscopy (RESPES) involves atomic processes of the type

$$3p^6 3d^n \rightarrow 3p^5 3d^{n+1} \rightarrow 3p^6 3d^{n-1}\varepsilon_k \ ,$$

for Cu, and processes of the type

$$\begin{aligned} 4d^{10}5p^6 4f^n 5d^m \rightarrow 4d^9 5p^6 4f^{n+1} 5d^m \rightarrow 4d^{10}5p^6 4f^{n-1} 5d^m \varepsilon_k \quad &\text{for } 4f \ , \\ \rightarrow 4d^{10}5p^6 4f^n 5d^{m-1}\varepsilon_k \quad &\text{for } 5d \ , \\ \rightarrow 4d^{10}5p^5 4f^n 5d^m \varepsilon_k \quad &\text{for } 5p \ , \end{aligned}$$

for La and Ba. The first step of the process is a photon absorption, $3p \rightarrow 3d$ for Cu and $4d \rightarrow 4f$ for La, Ba, leading to an intermediate state. The second step is a two-electron Koster-Kronig decay of the intermediate state, involving an Auger

matrix element of the Coulomb interaction, where ε_k labels the state of the photoelectron to be detected. Note that the final states can also be reached by a direct photoemission process in each case,

$$3d^n \rightarrow 3d^{n-1}\varepsilon_k ,$$

for Cu, and

$$4f^n \rightarrow 4f^{n-1}\varepsilon_k ,$$

$$5d^m \rightarrow 5d^{m-1}\varepsilon_k ,$$

$$5p^6 \rightarrow 5p^5\varepsilon_k ,$$

for La, Ba. Since the two processes add coherently, there can be quantum interference between them, leading to Fano-type line shapes.[47,48,51,52]

For La and Ba there are three possible processes that might be involved in the valence-band RESPES. Since n is nominally 0 for La and Ba, the $5d$ process might seem most likely, with the value of m rather uncertain since the $5d$ states are expected to be bandlike. However, experience with light rare earths[50] indicates that the Koster-Kronig processes for $4f$ and $5p$ electrons are much larger than that for $5d$, probably because the $5d$ states are much less localized. Thus the possibility cannot be dismissed that the RESPES is due to the admixture of $4f$ or even $5p$ states into the valence band. For Cu, the process cannot proceed if $n=10$ (Cu^{1+}). Also, it is shown below that $n=8$ (Cu^{3+}) is energetically prohibited, leaving $n=9$ (Cu^{2+}) as the valence state from which the resonance proceeds. It should be noted that a different mechanism than described above has been invoked for the weaker RESPES of the d^{10} state of Cu metal.[48]

Figure 2 shows the EDC's for $La_{1.8}Sr_{0.2}CuO_4$ sample No. 2 for $h\nu$ in the vicinity of the Cu $3p$ edge. The data for our La_2CuO_4 samples are essentially identical, except that the Fermi edge is not seen clearly. Peak C was discussed above. Peaks A, B, and D display resonant behavior, implying that they involve Cu $3d$ states. The resonance of the satellite $3d^8$ feature, peak D, is easily seen in Fig. 2, while that of peaks A and B is more clearly seen in Fig. 3. Figure 3 shows the photon energy dependences for emissions at binding energies labeled by the values of E_i. These curves are called constant initial-state CIS spectra, because they are taken by scanning the photon energy and the CMA energy E_{KE} together so that $E_i = h\nu - E_{KE}$ is maintained constant. The curves of Fig. 3 are the differences of the raw CIS data and smooth spline fits to the data which account approximately for the background photoemission cross-section dependences. For the $E_i = 0.5$ eV Fermi level curve, the intensity was so low that it was difficult to obtain a good spline fit, and this is probably the reason why the resonance appears slightly shifted relative to those of the other curves. There may also be some uncertainty in the magnitude of the Fermi-level resonance. The vertical scale is the same for all the curves. As a per-

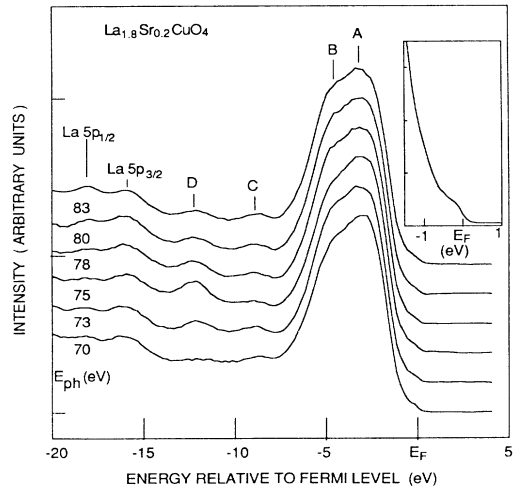

FIG. 2. Room-temperature valence-band EDC's for photon energies in the Cu $3d$ RESPES region for the UCSD $La_{1.8}Sr_{0.2}CuO_4$ sample of Fig. 1. Inset shows the detail of the Fermi-level region at a photon energy of 70 eV. Peak C is discussed in the text, and Peak D is the Cu d^8 satellite.

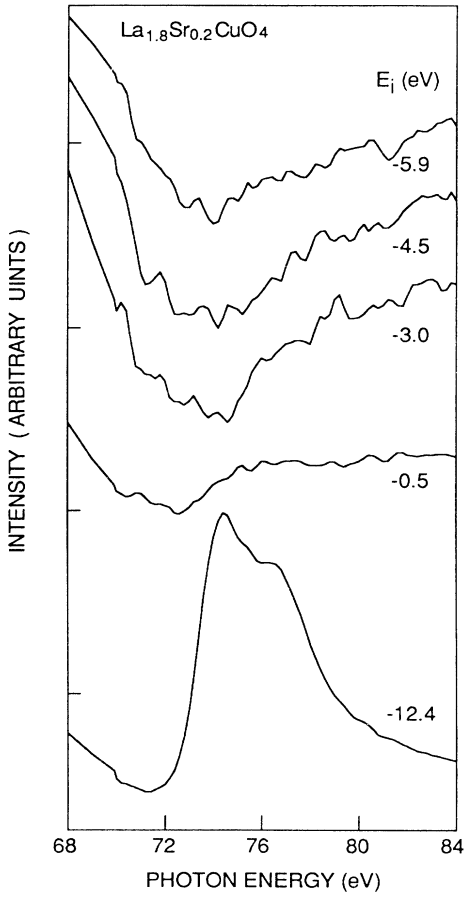

FIG. 3. CIS spectra in the Cu $3d$ RESPES region for various binding energies E_i of the valence-band spectra of Fig. 2. The spectra are the differences between raw data and a smooth spline fit to the data. The main band emission shows a resonance dip and the satellite emission shows a resonance peak as in CuO and Cu_2O. The vertical scale is arbitrary but the same for all the curves.

centage of the background, the satellite resonance is much larger than that for the main band because the satellite itself is quite weak. As is observed[38,39] for CuO, Cu_2O, and Ni compounds, the resonance shapes are Fano-like, with differing Fano q parameters such that peak D shows a resonance peak, while the main band features at smaller binding energy show a resonance dip. These differing dependences have been qualitatively explained for transition-metal compounds in theories[13,15,51] based on the cluster model of Sec. VII or the Anderson model with a ligand continuum.[53]

The Cu RESPES shows that both features A ($E_i = -3.0$ eV) and B ($E_i = -4.5$ eV) of Fig. 2 involve Cu $3d$ states. More important, the CIS taken for $E_i = -0.5$ eV, just above E_F, also shows resonance behavior. Although the absolute magnitude of the resonance is smaller than that of the other curves, it is a large fraction of the total intensity of the weak emission at E_F. This means that models for the superconducting and normal states should include the Cu $3d$ character at E_F.

As $h\nu$ is increased from the resonance region to 120 eV, the intensity of feature A decreases relative to that of feature B. This behavior can be seen for the more limited range of $h\nu$ in Fig. 2. It can be inferred that the oxygen contribution to feature A is larger than for feature B, since the photoemission cross section of oxygen decreases faster than that of Cu over this range of $h\nu$. The emission at E_F is too weak to draw conclusions about the presence or absence of oxygen states.

The presence at the Fermi level, and in the main band, of states associated with La can be inferred from the CIS curves of Fig. 4, which show the region of the La $4d$ absorption edge. To show the strength of the La resonance relative to that of the smoothly varying Cu and O background, the lower five curves have been normalized to change by the same amount over the energy range shown. The top curve has a different scale and is for the La $5p$ core-level emission. As observed for the RESPES of other La compounds,[54] the peaks in the spectrum are due to the three intermediate states of the configuration $4d^9 4f^1$ that can be reached by an electric-dipole absorption, $^3P_1$, $^3D_1$, and $^1P_1$. Most of the oscillator strength is in the $^1P_1$ state, as predicted theoretically, and the energies of the three states are in reasonable agreement with theoretical predictions.[55] For the main band CIS curves, the $^3P_1$ state is not observed, probably because of its small electric dipole matrix element. There are La-induced states everywhere in the main band, including the Fermi level. Thus the completely ionic picture in which all the La electrons are donated to states of Cu and O is too simple, as shown also by partial densities of state from band calculations.[44] The resonace line shapes are interesting in that the $^3D_1$ shape changes from a dip for the main band to a peak for the $5p$ core level, and the $^1P_1$ shape is a peak for all states but those just at E_F, where it is a dip. Detailed theoretical analysis using recent advances in RESPES theory[56,57] will be required to extract all the information latent in these data.

For $YBa_2Cu_3O_{7-\delta}$ the presence of Ba causes a problem for observing RESPES of the Cu valence-band satellite, as has been pointed out by others.[35,41] This is shown by

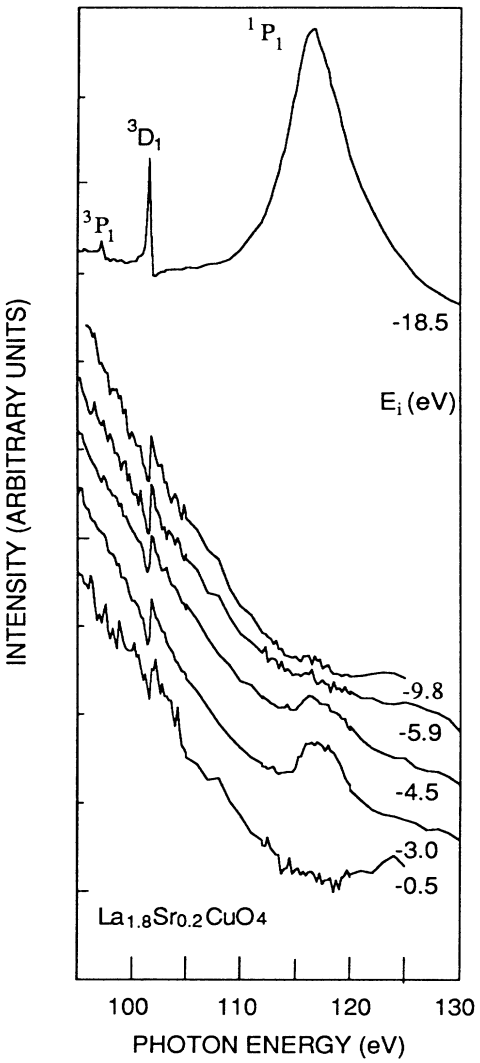

FIG. 4. CIS spectra in the La RESPES region for various binding energies E_i of the valence-band spectra of Fig. 2. The three allowed intermediate states of $4d^9 4f^1$ can be seen in the top spectrum for the La $5p$ level.

the EDC's in panel (b) of Fig. 5. Due to second-order light from the grating monochromator, there is emission from the intense Ba $4d$ core levels which happens to have the same kinetic energy as that of the Cu satellite emission due to the first order light. This second-order emission moves through the valence band, as shown by the pair of labeled peaks in the figure. As the photon energy decreases, the intensity of the second-order light decreases and so the second-order peaks become smaller. Since the second-order peaks cannot be entirely eliminated by filters placed after the monochromator, and since the filters considerably reduce the total signal, it was decided to measure the spectra without filters to obtain a very good signal-to-noise ratio, which enables the following correction procedure. The $h\nu = 80$ eV spectrum, where the second-order emission is well away from the valence-band

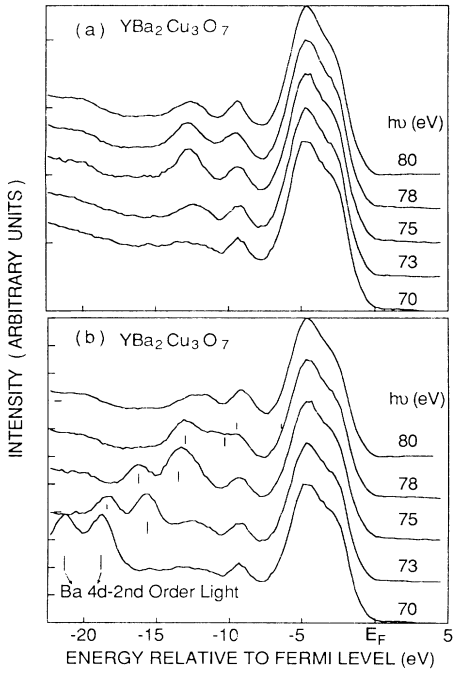

FIG. 5. Room-temperature valence-band EDC's for photon energies in the Cu $3d$ RESPES region for the $YBa_2Cu_3O_7$ SRI sample of Fig. 1, (a) corrected as described in the text, and (b) uncorrected for Ba $4d$ peaks due to second-order light.

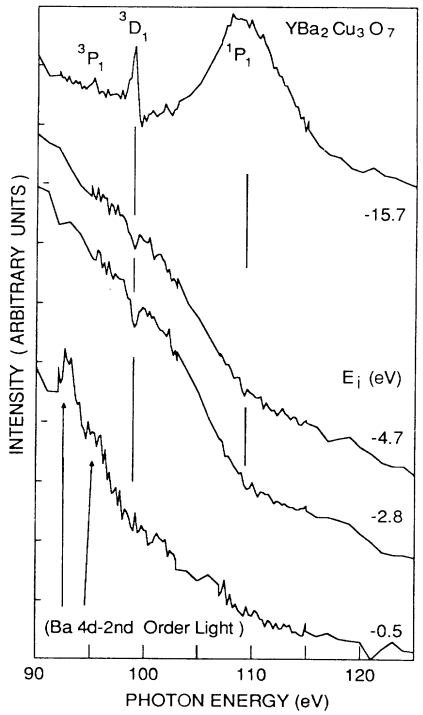

FIG. 6. CIS spectra in the Ba RESPES region for various binding energies E_i of the valence-band spectra of Fig. 5.

structure is fit as a sum of various peaks, including the two second-order peaks. The spectra for other photon energies are then fit, maintaining as a single entity the shape for the two second-order lines, but sliding it in energy and scaling it in amplitude. The curves of panel (a) result from subtracting the second-order line fits from the data. The procedure works well, and the resonance behavior of the satellite can easily be seen. CIS curves for the main bands are essentially the same as those of Fig. 3. Again, it appears that there are Cu $3d$ states very near the Fermi energy.

Figure 6 shows CIS curves for the range of $h\nu$ around the Ba $4d$ edge. The curves are scaled as described for Fig. 4. Structure due to Ba $4d$ emission induced by second-order light can be seen in the lowest curve. The top CIS spectrum for the Ba $5p$ emission shows the $4d^9 4f^1$ intermediate states and similar line shapes to those observed for the La materials, and for Ba metal.[58] The presence of Ba emission in the main band is shown by the middle two curves. The $^3D_1$ line shape differs for the $5p$ and main band emissions in the same way as found for the La material. However, in the region of the $^1P_1$ intermediate state, the main band always appears to show a resonance dip. The data are marginal with respect to the presence of Ba states near E_F. A full interpretation of these resonance effects probably must take account of the known complexities[59,60] of the Ba $4d$ absorption process.

The least-binding energy shoulder of the $YBa_2Cu_3O_{7-\delta}$ sample No. 2 of Fig. 1 shows an additional photon energy dependence relative to that of the higher binding-energy peak. As the photon energy increases from 40 through 75 eV, the shoulder decreases considerably, in the general fashion expected for the Cooper minimum in the cross section for Y $5d$ states. On this basis, the shoulder is assigned to Y states of some sort, as discussed further in Sec. VI.

V. Cu $2p$ AND OTHER XPS SPECTRA

Figure 7 shows the Cu $2p$ core-level spectra of our superconductor samples, as well as those of Cu and CuO. The upper three spectra were taken at Stanford, and the bottom three were taken at Xerox PARC. A La_2CuO_4 spectrum is shown for each as an indication that the binding energy calibrations in the two spectrometers are the same. The spectra consist of spin-orbit split $2p_{1/2}$ and $2p_{3/2}$ components, each of which has a main line and a satellite. In Sec. VI the separation and intensity ratios of the two $2p_{3/2}$ lines are analyzed using the Anderson model. The separation, 8.7 eV, is approximately equal to U_{cd}, the Coulomb interaction between the Cu $2p$ core hole and $3d$ electrons. For transition-metal compounds, $U_{dd}/U_{cd} \simeq 0.7$ has been found in other studies,[19] leading to a preliminary estimate of $U_{dd} \simeq 6$ eV, as pointed out by Fujimori, Takayama-Muromachi, Uchida, and Okai.[33] The chemical shift from Cu to CuO agrees with that of a previous measurement,[61] and it is significant that the chemical shifts of the superconducting samples are intermediate, indicating that the oxidation of Cu in these sam-

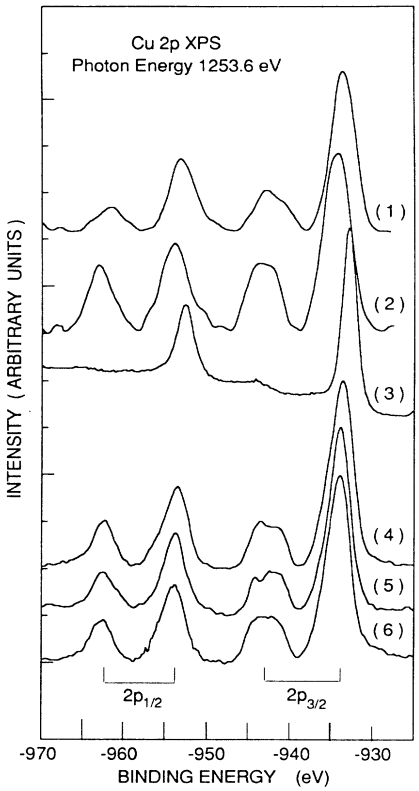

FIG. 7. Cu $2p$ XPS spectra for (1) Stanford La_2CuO_4, (2) CuO, (3) Cu, (4) UCSD La_2CuO_4, (5) UCSD $Cu_{1.8}Sr_{0.2}CuO_4$, and (6) UCSD $YBa_2Cu_3O_{7-\delta}$.

ples is less than that of CuO and providing strong additional evidence that Cu^{3+} does not occur. As pointed out in Sec. III, this conclusion is perfectly consistent with the large energy of the Cu d^8 state implied by the analysis of Sec. VII. The linewidths for Cu and CuO are also in agreement with previous results,[61] and those for the superconducting samples are intermediate between the two.

Other XPS core-level spectra were measured. The observation of the carbon $1s$ level has already been mentioned. The O $1s$ XPS spectra of all our samples show split peaks. Before cleaning the sample, the higher binding-energy peak is the larger, and after cleaning it becomes the smaller. This suggests that the higher binding-energy peak is not intrinsic, and is perhaps due to grain boundary oxides of the constituent elements. Possible intrinsic mechanisms for such a splitting could be the presence of the crystallographically inequivalent oxygen sites, or of two oxygen valence states. The first possibility is inconsistent with the observation that the intensity ratios of the two peaks vary and never correspond to the ratio of oxygen sites. The second seems unlikely in view of the fact that in NiO the charge fluctuations due to hybridization between Ni $3d$ and O $2p$ electrons produce splittings of the Ni $2p$ core lines, while the O $1s$ core line remains unsplit.[16] Another extrinsic possibility is CO trapped in the grain boundaries. Before cleaning of the La-containing samples, the La $3d$ lines show many peaks, and after cleaning they are split in much the same way as occurs in La_2O_3 due to La—O hybridization. Since La bonds to oxygen in the sample, the spectrum could be intrinsic, or could reflect some grain boundary oxide, or both, if the magnitudes of the splittings and chemical shifts in the two cases are comparable.

VI. CAVEATS FROM SAMPLE AND TIME DEPENDENCES OF SPECTRA

Time-dependent effects were observed in the RESPES spectra of our samples. For La_2CuO_4 and $La_{1.8}Sr_{0.2}CuO_4$ the effect was very slow and consisted of a decrease in the intensity of feature A relative to that of feature B in Fig. 2. This change first became noticeable after a time period of about three hours after fracturing or scraping the surface. Assuming oxygen emission contributes more to feature A than B, as indicated by the photon energy dependence pointed out in Sec. III, this could be explained by the hypothesis that oxygen leaves the sample slowly. However, another very interesting observation is that the La resonances of Fig. 4 also disappeared on the same time scale, suggesting a more complex process involving both La and O. After a fresh scrape or fracture, the original amplitude of peak A is restored, along with the La resonance.

For $YBa_2Cu_3O_{7-\delta}$ sample No. 2 of Fig. 1, a faster time dependence was observed for the least binding-energy shoulder. Within 3 h after a scrape or fracture this shoulder has almost disappeared so that the spectra of samples No. 1 and No. 2 became very similar. The speed is not dependent on the photon intensity, or energy, suggesting that the change is not radiation induced. The fact that sample No. 1 shows no shoulder, and yet the two samples have similar values of T_c, seems to imply that if the shoulder is intrinsic to the superconducting material, there is a mechanism for its change to be at least two orders of magnitude faster in one sample than another. An equally plausible possibility is that the shoulder is due to some grain boundary material present in sample No. 2 and not sample No. 1, and that the grain boundary material diffuses away from the surface with time, as is known to occur in some other polycrystalline materials. A possibility for the grain boundary material is Y_2O_3, because the method of preparing this sample is thought to yield Y-rich material. This hypothesis is also consistent with the Y character of the shoulder inferred from its $h\nu$ dependence, as mentioned in Sec. IV, and the split oxygen peaks mentioned in Sec. V.

At the moment, these kinds of effects must be taken as reminders that electron spectroscopy is a surface-sensitive measurement and is therefore especially susceptible to the kinds of effects that might be expected from ceramic samples of materials in which rapid oxygen diffusion is known to occur. On the other hand, the XPS spectra from the same samples were found to be very stable as a function of time, perhaps because the XPS sampling depth is greater than in the soft x-ray valence-band spectra due to the considerable differences in the elastic escape depth for the kinetic energies of electrons in the two experiments. With the passage of time, as more experience is accumulated

with samples of this type, and when single-crystal material is measured, these issues will be clarified. In the meantime, *the analysis to follow focuses on features of the spectra which occur in all samples and which are not time dependent.*

VII. CLUSTER CONFIGURATION INTERACTION MODEL OF THE ANDERSON HAMILTONIAN

The simplest version of the Anderson model which retains the various charge fluctuation processes is the local cluster model applied first to Cu compounds by Sawatzky and co-workers.[12-14] In this approach a $(CuO_6)^{10-}$ cluster is regarded as a separable unit and its electronic structure is described by configuration interaction. In essence it is an Anderson impurity Hamiltonian description of the Cu $3d$ electrons hybridized to the oxygen $2p$ states, but neglecting the $2p$ bandwidth. Because the model is simple, it is easy, and useful for the discussion, to reproduce the analysis of Refs. 12 and 13 below.

Figure 8 shows an energy-level diagram of the configurations included in treating the ground state and the states reached in $2p$ photoemission, plus the effect of hybridization. The ground state is a linear combination of properly symmetrized d^9 and $d^{10}L$ configurations, where L denotes a hole of appropriate symmetry relative to filled ligand O $2p$ states. Similarly, the final states reached in $2p$ photoemission are described as linear combinations of symmetrized $2p^5d^9$ and $2p^5d^{10}L$ configurations. Evidence that these are indeed the appropriate basis states is provided by the different line shapes of the $2p_{1/2}$ and $2p_{3/2}$ satellites, shown in Fig. 7. In the cluster model, the satellites are mainly $2p^5d^9$ states, and it has been shown[12] that the difference in line shapes is well accounted for by the different term splittings predicted for the $2p^5_{1/2}d^9$ and $2p^5_{3/2}d^9$ configurations. For simplicity these crystal-field and term splittings of the manifolds are neglected here. The Hamiltonian for the initial and final states is then a 2×2 matrix:

$$\begin{pmatrix} E_1 & T \\ T & E_2 \end{pmatrix} . \tag{1}$$

The off-diagonal element is defined as the transfer integral $T\equiv\langle d^9|H|d^{10}L\rangle$. For the ground state the diagonal elements are

$$E_1=0 , \tag{2}$$

$$E_2=\Delta\equiv\langle d^{10}L|H|d^{10}L\rangle-\langle d^9|H|d^9\rangle , \tag{3}$$

and for the core-hole states the diagonal elements are

$$E_1=E_{2p}+\Delta , \tag{4}$$

$$E_2=E_{2p}+U_{cd} , \tag{5}$$

where in each case $|1\rangle$ is the lower energy state shown in Fig. 8. U_{cd} is a repulsive interaction between the $2p$ core hole and the $3d$ hole of the $3d^9$ configuration, so that for $U_{cd}>\Delta$, the core hole stabilizes the $d^{10}L$ configuration, as shown in Fig. 8. The quantity Δ can be described as a sum of the energies of the processes of adding a d electron and making a ligand hole,

$$\Delta=(\langle d^{10}L|H|d^{10}L\rangle-\langle d^9L|H|d^9L\rangle) + (\langle d^9|H|d^9\rangle-\langle d^9L|H|d^9L\rangle)\equiv E_d+E_L , \tag{6}$$

with an obvious identification of terms.

The eigenvalues of Eq. (1) for the ground state are

$$E_{\text{ex,g.s.}}=\tfrac{1}{2}\Delta\pm\tfrac{1}{2}\sqrt{\Delta^2+4T^2} , \tag{7}$$

and for the core-hole states are

$$E_{s,m}=E_{2p}+\tfrac{1}{2}\Delta\pm\tfrac{1}{2}\sqrt{(\Delta-U_{cd})^2+4T^2} . \tag{8}$$

The corresponding eigenfunctions for Eq. (7) can be written

$$|\text{ex}\rangle=\sin\theta|d^9\rangle+\cos\theta|d^{10}L\rangle , \tag{9}$$

$$|\text{g.s.}\rangle=\cos\theta|d^9\rangle-\sin\theta|d^{10}L\rangle , \tag{10}$$

with

$$\tan(2\theta)=2T/\Delta , \tag{11}$$

where g.s. denotes the ground state and ex the excited state. The core-hole eigenfunctions have the same form as Eqs. (9) and (10) with

$$\tan(2\Phi)=2T/(\Delta-U_{cd}) . \tag{12}$$

From Eqs. (7) and (8) the energy separation of the satellite and main core lines is

$$\delta E(2p)=E_s-E_m=\sqrt{(\Delta-U_{cd})^2+4T^2} . \tag{13}$$

In the sudden approximation, the intensity ratio of the satellite and main core lines is

$$I_s/I_m(2p)=(\langle g|s\rangle/\langle g|m\rangle)^2 = \frac{(\cos\theta\sin\Phi-\sin\theta\cos\Phi)^2}{(\cos\theta\cos\Phi+\sin\theta\sin\Phi)^2} . \tag{14}$$

Equations (11)–(14) give two relations for the three parameters T, Δ, and U_{cd}, with $I_s/I_m(2p)$ and $\delta E(2p)$ being determined experimentally. The analysis is done here for the $2p_{3/2}$ line because certain interference effects[20] alter the intensity ratio for the $2p_{1/2}$ line. For our samples these data are listed in Table I, and lead to the results for Δ and U_{cd} as a function of T shown in Fig. 9. It is apparent that U_{cd} is nearly constant from sample to sample,

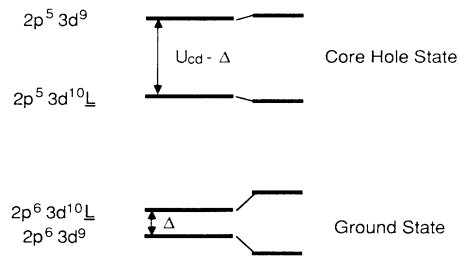

FIG. 8. Energy-level diagram for configurations of the cluster model description of the initial and final states for Cu $2p$ XPS. The changes in splittings are due to hybridization.

TABLE I. Experimental quantities for the three materials, as defined in the text. All energies are given in eV.

	La_2CuO_4	$La_{1.8}Sr_{0.2}CuO_4$	$YBa_2Cu_3O_7$ (Sample 1)	CuO
$\delta E(2p)$	8.5	8.9	8.8	8.9
$I_s/I_m(2p)$	0.33	0.34	0.35	0.45
W(VB)	4.4	4.7	4.8	5.0
δE(VB)	8.6	8.5	8.2	8.6
I_s/I_m(VB)	0.02	0.02	0.03	0.20
E_m(VB)	−3.8	−3.9	−4.2	−4.3
E_s(VB)	−12.4	−12.4	−12.7	−12.9

and does not provide any criterion for choosing T, and hence Δ. However, stability considerations described below lead to choosing Δ positive, which implies $T > 2.2$ eV.

It remains to discuss the valence band in the cluster model. The final states of valence-band photoemission are described as linear combinations of d^8, d^9L, and $d^{10}L^2$ states. For inverse photoemission there is only one state, d^{10}. Figure 10 is an energy-level diagram of the configurations with and without the effect of hybridization. Using the standard expression from the Anderson or Hubbard Hamiltonians,

$$E(d^n) = -n\varepsilon_d + \tfrac{1}{2}n(n-1)U \ , \tag{15}$$

where $-\varepsilon_d$ is the single-particle d-orbital energy, and the definitions of E_d and E_L from Eq. (6), it follows that relative to $E(d^9)\equiv 0$,

$$E(d^9L) = E_L \ , \tag{16}$$

$$E(d^{10}L^2) = 2E_L + E_d = E_L + \Delta \ ,$$

$$E(d^8) = -E_d + U = E_L + U - \Delta \ . \tag{17}$$

Adding the constant $\Delta - E_L$ to each diagonal element, the Hamiltonian for the valence-band photoemission final state is then a 3×3 matrix,

$$\begin{pmatrix} \Delta & T\sqrt{2} & T\sqrt{2} \\ T\sqrt{2} & 2\Delta & 0 \\ T\sqrt{2} & 0 & U \end{pmatrix} \ , \tag{18}$$

where the factor of $\sqrt{2}$ accounts for the degeneracy associated with 2 d holes or 2 ligand holes, in the spirit of the $1/N$ theory[50,56] of the Anderson Hamiltonian; i.e., $T_{\text{eff}} \simeq T\sqrt{N}$, where N is the degeneracy. The eigenvalues of Eq. (18) give the relative separations of the energy levels of the valence band. The largest eigenvalue corresponds to the satellite, and if $U \gg \Delta$, as turns out to be the case here, its eigenstate is mainly d^8. The main valence-band peak must coincide with the centroid of the energies of the states derived from d^9L and $d^{10}L^2$. These are split by approximately $(\Delta^2+8T^2)^{1/2}$, which should then be roughly the width W(VB) of the main peak. The separation between the centroid and the largest eigenvalue should give the experimental separation δE(VB) between the energy of the main valence-band peak, E_m(VB), and that of the satellite, E_s(VB). The experimental values of W(VB), δE(VB), E_m(VB), and E_s(VB) are listed in Table I. From the values of W(VB), it is clear that T and Δ should be chosen as small as possible, consistent with the condition above from the $2p$ spectra that $T > 2.2$ eV. For given values of T and Δ, the eigenvalues and eigenvectors of Eq. (18) can be found as a function of U, and U can then be chosen to give δE(VB). Figure 11 shows an example of the eigenvalue variation for the case $T = 2.4$ eV, $\Delta = 0.3$ eV.

One final condition which must be met in choosing parameter values concerns E_L and E_d and the stability of the ground state. A discussion of this condition has not been

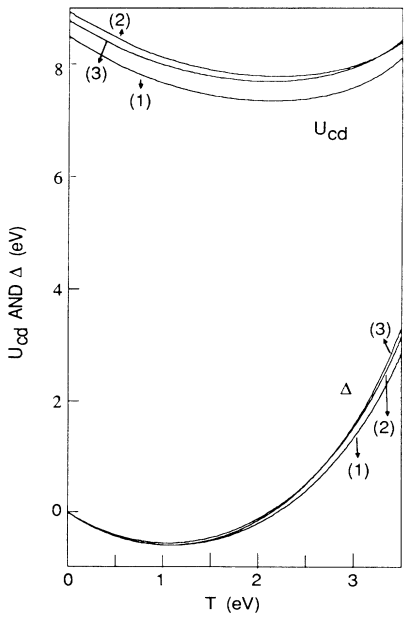

FIG. 9. The variation of U and Δ with T in the cluster model for the experimental values of the Cu $2p$ satellite to main band intensity ratio and separation for (1) La_2CuO_4, (2) $La_{1.8}Sr_{0.2}CuO_4$, and (3) $YBa_2Cu_3O_{7-\delta}$.

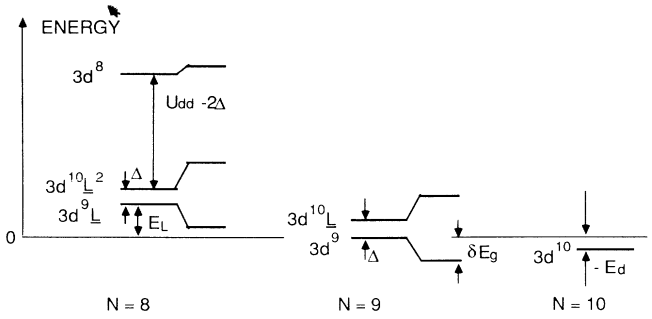

FIG. 10. Energy-level diagram for configurations of the cluster model description of the ground-state ($N=9$), valence-band photoemission final states ($N=8$), and BIS final states ($N=10$). The changes in splittings are due to hybridization.

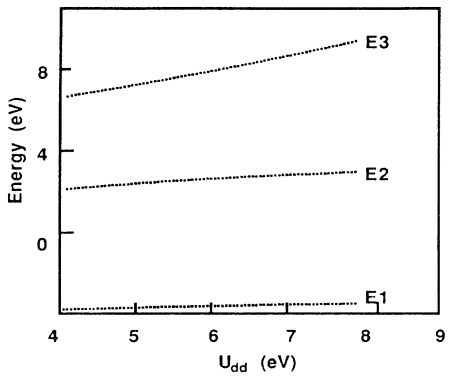

FIG. 11. U dependence of the photoemission final-state eigenvalues for $La_{1.9}Sr_{0.2}CuO_4$, $T=2.4$ eV, and $\Delta=0.3$ eV. U is chosen to make the separation of the $E1/E2$ centroid and $E3$ equal to the separation of the main and satellite peaks of the valence-band photoemission spectrum.

given in the literature before. Referring to Fig. 10, and recalling the definition of the diagonal elements of (18), the valence-band excitation energies, relative to the $N=9$ ground state, are given by adding to the eigenvalues of Eq. (18) the quantity $(E_L-\Delta+\delta E_{\text{g.s.}})$ where $\delta E_{\text{g.s.}}$ denotes the hybridization shift of the ground state, given by Eq. (7). The three excitation energies are $E_{m1}(\text{VB})$, $E_{m2}(\text{VB})$, and $E_s(\text{VB})$, with an obvious notation. Similarly the excitation energy for adding an electron is given by $(E_d+\delta E_{\text{g.s.}})$. This excitation could be observed by BIS, so this energy is denoted E_{BIS}. For the system to be stable these excitation energies must be zero or positive. The stability conditions implied by $E_{\text{BIS}}\geq 0$, $E_{m1}(\text{VB})\geq 0$, and Eq. (6) can be written as a condition on E_L,

$$\Delta+\sqrt{\Delta^2+4T^2}\geq 2E_L\geq\sqrt{\Delta^2+8T^2}-\sqrt{\Delta^2+4T^2}\ . \tag{19}$$

If $\Delta=0$, Eq. (19) gives $T\geq E_L\geq(\sqrt{2}-1)T$, and if $T=0$, Eq. (19) gives $(\Delta+|\Delta|)/2\geq E_L\geq 0$. The latter result shows that for $T=0$, if $\Delta<0$, then $E_L=0$, which leads to $E_{\text{BIS}}=E_{m1}(\text{VB})=0$ [also E_{gap} defined in Eq. (23) below equals 0], so the model mimics a mixed-valent metal for this case. Taking the experimental Fermi level to coincide with the theoretical ground state, E_L must also be chosen to align the eigenvalue spectrum with the experimental quantities $E_m(\text{VB})$, $E_s(\text{VB})$. Because $E_m(\text{VB})$ in Table I is rather large, E_L must also be rather large. In order to insure that Eq. (19) is satisfied, one must try to choose T and Δ as large as possible without compromising the agreement with $W(\text{VB})$ too greatly.

The satellite intensity can also be calculated as was done for the core-level case. Denoting by a and b, respectively, the coefficients of the $|d^9\rangle$ and $|d^{10}L\rangle$ states in Eq. (10) and expressing the eigenfunctions of (18) as

$$|i\rangle=a_i|d^8\rangle+b_i|d^9L\rangle+c_i|d^{10}L^2\rangle\ , \tag{20}$$

where $i=1,2,3$, the various intensities for d photoemission are given by

$$I_i=(aa_i+bb_i)^2\ . \tag{21}$$

Of particular interest is the ratio $I_s/I_m(\text{VB})$ of the satellite to main band intensity $(I_m=I_{m1}+I_{m2})$, the experimental values of which are listed in Table I. These experimental values are derived from spectra taken with $h\nu$ away from the Cu $3p$ resonance. $I_s/I_m(\text{VB})$ is found to be quite sensitive to the values of T and Δ, as described in Sec. IX. Qualitatively, since all the intensity would be in the satellite for no hybridization mixing, i.e., $T=0$, and since I_s/I_m in Table I is very small, large T and small Δ are favored.

Table II shows parameter values chosen as a compromise to satisfy all the conditions set forth above. They are similar to those of Ref. 33. The table also shows the resulting calculated values of $\delta E_{\text{g.s.}}$, $E_{m1}(\text{VB})$, $E_{m2}(\text{VB})$, $E_s(\text{VB})$, and $I_s/I_m(\text{VB})$. The last four of these quantities can be compared with the corresponding experimental values in Table I. The greatest failing is that a value of T large enough to satisfy the stability conditions causes the two lowest eigenvalues to be more widely split than the experimental valence bandwidth. The small values of E_{BIS} in the table show that for these parameters the system is close to instability. The last two table entries are the number of d electrons, n_d, given from Eq. (10) by

$$n_d=9\cos^2\theta+10\sin^2\theta\ , \tag{22}$$

and the theoretical energy gap of the system,

$$E_{\text{gap}}=E_{\text{BIS}}+E_{m1}(\text{VB})\ . \tag{23}$$

The values of n_d reflect the large hybridization mixing. E_{gap} is larger than Δ because of the hybridization shifts. As pointed out[16] for NiO, E_{gap} is much smaller than U,

TABLE II. Model parameters and quantities for the three materials measured, and for CuO. Energies are in eV. The various symbols are defined in the text. $E_s(\text{VB})$ and $E_{m1,2}(\text{VB})$ are relative to the theoretical Fermi level and can be compared to the experimental valence-band quantities in Table I.

	La_2CuO_4	$La_{1.8}Sr_{0.2}CuO_4$	$YBa_2Cu_3O_7$ (Sample 1)	CuO
U_{cd}	7.4	7.8	7.8	8.4
T	2.3	2.4	2.5	2.4
Δ	0.3	0.3	0.5	1.0
U	6.5	6.1	6.5	7.3
E_L	2.25	2.3	2.6	2.7
E_d	−1.95	−2.0	−2.1	−1.7
δE_g	2.15	2.25	2.2	1.95
$E_{m1}(\text{VB})$	0.8	0.65	0.9	1.05
$E_{m2}(\text{VB})$	6.8	6.85	7.5	7.5
$E_s(\text{VB})$	12.3	12.25	12.8	12.8
$I_s/I_m(\text{VB})$	0.03	0.03	0.04	0.16
E_{BIS}	0.2	0.25	0.2	0.25
n_d	9.4	9.5	9.4	9.4
E_{gap}	1.0	0.9	1.1	1.3

and has more the energy of a charge-transfer gap than a Hubbard gap. It can perhaps be regarded[16,17] as an effective U, strongly screened by hybridization, in the sense that it separates the minimum energies for adding and removing $3d$ electrons. Section IX gives some further discussion of the implications of these energy parameters.

VIII. MAGNETIC INTERACTION ENERGY

The cluster model can also be used to study the magnetic coupling that arises between two Cu ions due to virtual charge fluctuations. An important point, shown by Geertsma[62] and possibly others in the earlier superexchange literature, and used by Zaanen and Sawatzky[63] to discuss the superexchange interaction in NiO, CoO, FeO, and MnO, is that both polar and charge-transfer fluctuations lead to a magnetic interaction. Only the contribution due to the polar fluctuations has the usual Anderson superexchange[64] form. For the discussion, a compact analysis patterned after that of Ref. 63 is given below.

For present purposes it suffices to consider cubic symmetry and a three-center linear model with a central ligand atom and two cations. This neglects the splitting of the three-quarters-filled cubic e_g orbital of d^9 and the anisotropy of the hybridization matrix elements, but the error is probably not greater than that associated with the uncertainties of the spectroscopic parameters. Relative to filled ligand-p and cation-d states, the ground state is a linear combination of states with two holes, e.g., configurations like $d^9p^6d^9$, $d^{10}p^5d^9$, etc. Figure 12 shows the disposition of up and down spin holes in the various ferromagnetic and antiferromagnetic states that are possible. The states are labeled by numbers, and a bracket sign denotes pairs of states for which the symmetric normalized linear combination of states is to be used. It is convenient for extracting the exchange interaction to work with antisymmetrized states which are eigenfunctions of total spin. Thus, for example, the wave functions for singlet antiferromagnetic states 2 and 3 are

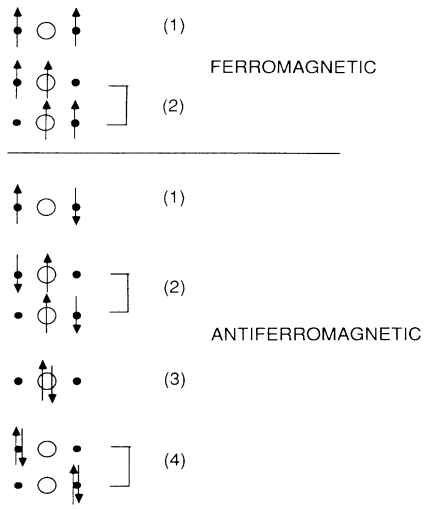

FIG. 12. Configurations used for the cluster calculation of the magnetic exchange coupling J. The solid dots are two Cu sites and the open circle is an intervening oxygen site in a linear geometry. The arrows show the spin of holes relative to filled Cu $3d$ and O $2p$ states. The symmetric combination of bracketed pairs is used, and the numbering corresponds to the rows and columns of the Hamiltonian matrices in the text. The charge-transfer and polar contributions to J arise from antiferromagnetic configurations (3) and (4), respectively.

$$\Phi_2(\mathrm{AF})=(1/\sqrt{8})[\Phi_a(r_1)\Phi_L(r_2)+\Phi_L(r_1)\Phi_a(r_2)+\Phi_b(r_1)\Phi_L(r_2)+\Phi_L(r_1)\Phi_b(r_2)][\alpha(1)\beta(2)-\beta(1)\alpha(2)]\ , \quad (24)$$

$$\Phi_3(\mathrm{AF}=(1/\sqrt{2})\Phi_L(r_1)\Phi_L(r_2)[\alpha(1)\beta(2)-\beta(1)\alpha(2)]\ , \quad (25)$$

and for the triplet ferromagnetic state 1 is

$$\Phi_1(\mathrm{AF})=(1/\sqrt{2})[\Phi_a(r_1)\Phi_b(r_2)-\Phi_b(r_1)\Phi_a(r_2)]\alpha(1)\alpha(2)\ , \quad (26)$$

where the indices 1,2 label the two holes, a,b label the left and right metal ion, L labels the ligand, and α,β are eigenstates of S^2 and S_z for $S=\frac{1}{2}$. For cubic symmetry, the σ-bonding hybridization matrix element $\langle L|H|a\rangle = \langle L|H|b\rangle$ is[64] $T_\sigma = T/\sqrt{3}$, and from Fig. 12 and the expressions of the previous section, it is apparent that the Hamiltonian for the antiferromagnetic cluster is

$$\begin{array}{c} |1\rangle \quad |2\rangle \quad |3\rangle \quad |4\rangle \\ \begin{pmatrix} 0 & T_\sigma\sqrt{2} & 0 & 0 \\ T_\sigma\sqrt{2} & \Delta & 2T_\sigma & T_\sigma\sqrt{2} \\ 0 & 2T_\sigma & 2\Delta & 0 \\ 0 & T_\sigma\sqrt{2} & 0 & U \end{pmatrix} \end{array}, \quad (27)$$

and for the ferromagnetic cluster is

$$\begin{array}{c} |1\rangle \quad |2\rangle \\ \begin{pmatrix} 0 & T_\sigma\sqrt{2} \\ T_\sigma\sqrt{2} & \Delta \end{pmatrix} \end{array}. \quad (28)$$

The off-diagonal zeros in Eq. (27) occur between states in which more than one electron has been transferred. The nonzero off-diagonal elements H_{23} and H_{24} of Eq. (27) differ by a factor of $\sqrt{2}$ from those of Ref. 63 due to the use of the antisymmetrized triplet and singlet wave functions of Eq. (24)–(26). For eigenstates of total angular momentum, the effective interaction $-J\mathbf{S}_a\cdot\mathbf{S}_b$ is diagonal and the singlet-triplet energy difference is J.

Defining $E_0(\mathrm{F})$ and $E_0(\mathrm{AF})$ to be the ground-state energies of the ferromagnetic and antiferromagnetic clusters, J is then given by

$$J=E_0(\mathrm{AF})-E_0(\mathrm{F}) \ . \tag{29}$$

The two ground-state energies satisfy the relations

$$E_0(\mathrm{F})-\frac{2T_\sigma^2}{E_0(\mathrm{F})-\Delta}=0 \ , \tag{30}$$

$$E_0(\mathrm{AF})-\frac{2T_\sigma^2}{E_0(\mathrm{AF})-\Delta-4T_\sigma^2/[E_0(\mathrm{AF})-2\Delta]-2T_\sigma^2/[E_0(\mathrm{AF})-U]}=0 \ . \tag{31}$$

Physical insight is gained by considering the case where $\Delta,U\gg E_0(\mathrm{F,AF})$ and $T_\sigma/\Delta,T_\sigma/U\ll 1$. Then these expressions become

$$E_0(\mathrm{AF})\simeq-\frac{2T_\sigma^2}{\Delta}\left[1+\frac{2T_\sigma^2}{U\Delta}\right] \ , \tag{32}$$

$$E_0(\mathrm{F})\cong-\frac{2T_\sigma^2}{\Delta}\left[1-\frac{2T_\sigma^2}{\Delta^2}\right] \ , \tag{33}$$

so that J is given by

$$J\simeq-4t_\sigma^2(\Delta^{-1}+U^{-1}) \ , \tag{34}$$

where the effective transfer integral t_σ for hopping from metal site to metal site is defined as

$$t_\sigma=T_\sigma^2/\Delta \ . \tag{35}$$

In addition to the polar term involving U, which has the form of the usual Anderson superexchange,[64] there is a term involving Δ. When $\Delta\ll U$, as is the case here, this term will dominate. As discussed elsewhere,[16,17] it is not clear precisely how to map this picture for J onto a Hubbard model for hybridized $3d$ states, in which t_σ and U, but not Δ, appear explicitly;[17] this is especially true if Δ is very small. One possible ansatz,[16,17] pointed out above, is to regard Δ, or perhaps E_{gap}, as the U of the Hubbard Hamiltonian, when $\Delta,E_{\mathrm{gap}}\ll U$ of the Anderson Hamiltonian.

For the values of T and Δ determined here, the approximations leading to Eq. (34) are not valid and so J has been determined by numerically diagonalizing Eq. (27), with the results $|J|\simeq 1.5$ eV shown in Table III. The uncomfortably large value of $|J|$ is due to the small value of Δ and the large value of T_σ. From Eq. (34) $|J|$ is expected to vary rapidly with changes in T_σ,Δ. For example, for $YBa_2Cu_3O_7$, if T_σ and Δ are decreased and increased, respectively, by 100%, $|J|$ is 0.3 eV. The value of T_σ depends on that of T, which has uncertainty, and on the relation between them, which will change because the symmetry of the actual crystal is lower than cubic. If the magnetic coupling involves only the $d_{x^2-y^2}$ orbitals in the plane of the four nearest oxygen neighbors, then according to Table II of Ref. 64 the value of T_σ would be reduced by a factor of $\sqrt{3/2}$ from the one used here, which is for coupling of two d_{z^2} orbitals along the z axis.

TABLE III. Model quantities relevant to magnetic interaction. All quantities are in eV, and symbols are defined in the text. The large magnitudes of J result from the combination of large T and small Δ. J varies rapidly with T,Δ. For example, as discussed in the text, a 100% increase in Δ and decrease in T gives for $YBa_2Cu_3O_7$, $J=-0.5$ eV, and for CuO, $J=-0.09$ eV.

	La_2CuO_4	$La_{1.8}Sr_{0.2}CuO_4$	$YBa_2Cu_3O_7$ (Sample 1)	CuO
E_0 (AF)	−3.1	−3.2	−3.2	−2.6
E_0 (F)	−1.7	−1.8	−1.8	−1.5
J	−1.4	−1.5	−1.4	−1.1
t_σ	5.9	6.4	4.2	1.9

Given the crudeness of the model, and the uncertainty of the parameters, the estimate for J has no more than order-of-magnitude significance. Nonetheless, even the smaller estimate is considerably larger than typical Néel temperatures for antiferromagnetic copper oxides. It is, however, the order of magnitude of J that has been inferred[25] from applying[24] the resonating-valence-bond theory to La_2CuO_4 materials, although the underlying virtual charge fluctuations invoked are not fully equivalent.

IX. DISCUSSION OF THE MODEL RESULTS

The values of the model parameters T and Δ obtained here must be regarded as rough estimates. The lack of a reliable BIS spectrum greatly limits the certainty with which the model parameters are known. In particular, a clearly identifiable $d^9\rightarrow d^{10}$ BIS peak would fix the values of E_{gap} and Δ, as could be done in the case of NiO[16]. There is also evidence that the values of T and Δ needed to describe core-level spectra can be somewhat different from those for valence-band spectra. One suggestion[19,20] is that T may be larger in the presence of the core hole. If the relation between T and Δ given in Fig. 9 is ignored, it is possible to find a range of parameter values which give the experimental values of Table I for $W(\mathrm{VB})$, $\delta E(\mathrm{VB})$, $E_m(\mathrm{VB})$, and $E_s(\mathrm{VB})$ and satisfy the stability relation in Eq. (19). However, the values of $I_s/I_m(\mathrm{VB})$ are then in very poor agreement with experiment. For example, in the case of $YBa_2Cu_3O_{7-\delta}$, for (T,Δ), the range is from (1.65,1.0) to (0,4.8), in eV, and $I_s/I_m(\mathrm{VB})$ calculated for the largest T is 0.6, an order of magnitude too large. For smaller T and larger Δ the agreement is even worse. Also, these smaller T values lead to values of $U>9$ eV because the hybridization shift of the valence-band satellite is much less. A value of $U>U_{cd}$ is implau-

sible. Thus it seems likely at the moment, in the absence of good BIS information on the unfilled Cu states, that the trend of a small Δ and a large T is roughly correct.

Estimates of model parameters for CuO led to the placement of this material in the region B of the generalized phase diagram of Ref. 18, i.e., the region of charge-transfer insulators. Analyzing our data and that[39,61] in the literature for CuO in the same way as for the superconducting copper oxides leads to the set of values given in Tables I–III. These would suggest that CuO is in region B, but is close to region C' of the phase diagram, where $E_{\rm gap}$ is comparable to T. The magnitude of J is very large compared to the CuO Néel temperature $T_N = 230$ K.[65] Increasing Δ and decreasing T_σ by 100% yields $J = 0.09$ eV, which is more reasonable, but still large. This suggests either that our J values should be regarded as suspiciously large, or that the resonating valence-bond model, or some other picture, should be applied to CuO in the same way[24,25] as for the superconducting oxides. The fact that the parameters account well for the much larger value of I_s/I_m(VB) of CuO relative to that of the other Cu oxides gives considerable credence to the T,Δ values.

The parameter values of the superconducting oxides suggest that they are in region C' of the phase diagram of Ref. 18. For this region, the cluster model is far too crude. The first improvement is to treat the ligand states, e.g., the d^9L states, as a continuum, as was done in Ref. 18. This is important because T is comparable to the oxygen bandwidth, and so the effects of the sharp states, e.g., d^8, interacting with the continuum will be very important in determining the band gap and the nature of the states near the top of the valence band. These states involve the mixing of two continua, for d^9L and $d^{10}L^2$, so there are Cu $3d$ valence fluctuations and correlated Cu $3d$ and O $2p$ occupations. There is additionally the mixing of the d^9L continuum with the d^8 sharp state. The considerable region of low density of states between the Fermi level and the first valence-band peak poses a serious problem. In the cluster model, it leads to the large value of E_L. In the impurity model with continuum ligand states the $3d$ spectral weight distribution due to hybridization with a sharp state typically gives a peak at the top of the continuum band, so it is not likely that the region of low spectral weight near E_F can be obtained from this model.[66] Indeed, the origin and nature of this low density-of-states region remains an important issue for additional clarification, beyond our finding here of a considerable Cu $3d$ contribution. For example, it cannot yet be ruled out that these are defect states associated with off-stoichiometry. Related to this is the current uncertainty in the magnitude of the intrinsic gap of the stoichiometric materials.

An equally serious consideration is that, with Δ very small, or perhaps even negative, and with T larger than Δ, there should be sizable lattice effects that require the lattice Anderson Hamiltonian. A clear sign that this is so is provided by the breakdown of the perturbation expressions for J and its large magnitude. Equivalently, from Eq. (34) the d-d hopping parameter t_σ is found to be very large, as shown in Table III. Fujimori, Takayama-Muromachi, and Uchida[67] have discussed the possibility of an analogy to the situation in cerium,[50] in which Kondo-type spin fluctuations dominate the low-energy physics. For the parameters found here, the role of charge fluctuations is likely to be the more important issue. As Δ goes to zero the virtual charge fluctuations become real, and one has[16,17] the difficult situation, like that of the mixed valence in TmSe or SmB_6, where lattice effects are known to be important in giving electrically insulating behavior,[68] even though T is much smaller. It seems possible that such considerations may be relevant to the issue of the origin of the low density-of-states region near E_F.

Thus we are left with the situation that the mechanism for the high T_c must probably be found in the same basic model that has made the heavy-Fermion problem so difficult, although the parameter range of the model is not the same, and there is, presumably, a gap at E_F in the continuum density of states of the stoichiometric materials.

ACKNOWLEDGMENTS

We are very thankful for numerous helpful discussions with C. Herring and G. A. Sawatzky. C. K. Shih graciously helped with the Stanford XPS measurements. The Stanford Synchrotron Radiation Laboratory and the work at Los Alamos National Laboratory are supported by the U.S. Department of Energy. Research support by the U.S. National Science Foundation through Low Temperature Physics Grant No. DMR-8411839 (J.W.A, J.S.K, M.B.M, and M.S.T.), and through the National Science Foundation-Materials Research Laboratory Program at the Center for Materials Research at Stanford University, is gratefully acknowledged.

*Present address: Physics Department, University of Michigan, Ann Arbor, Michigan 48109-1120.

[1] J. G. Bednorz and K. A. Müller, Z. Phys. B **64**, 189 (1986).

[2] H. Takagi, S. Uchida, K. Kitazawa, and S. Tanaka, Jpn. J. Appl. Phys. Pt. 2 **26**, L1 (1987); Jpn. J. Appl. Phys. Pt. 2 **26**, L123 (1987).

[3] R. J. Cava, R. B. van Dover, B. Batlogg, and E. A. Reitman, Phys. Rev. Lett. **58**, 408 (1987).

[4] J. M. Tarascon, L. H. Greene, W. R. McKinnon, G. W. Hull, and T. H. Geballe, Science **235**, 1373 (1987).

[5] J. D. Jorgensen, H.-B. Schüttler, D. G. Hinks, D. W. Capone II, H. K. Zhang, M. V. Brodsky, and D. J. Scalapino, Phys. Rev. Lett. **58**, 1024 (1987).

[6] M. K. Wu, J. R. Ashburn, C. J. Torng, P. H. Hor, R. L. Meng, L. Gao, S. J. Huang, Y. Q. Wang, and C. W. Chu, Phys. Rev. Lett. **58**, 908 (1987).

[7] R. J. Cava, B. Batlogg, R. B. van Dover, D. W. Murphy, S. Sunshine, T. Siegrist, J. P. Remeika, E. A. Rietman, S. Zahurak, and G. P. Espinosa, Phys. Rev. Lett. **58**, 1676 (1987).

[8]Sung-ik Lee, John P. Golben, Sang Young Lee, Xiao-Dong Chen, Yi Song, Tae W. Noh, R. D. McMichael, J. R. Gaines, D. L. Cox, and B. R. Patton, Phys. Rev. B **36**, 2417 (1987).
[9]P. M. Grant, R. B. Beyers, E. M. Engler, G. Lim, S. S. P. Parkin, M. L. Ramirez, V. Y. Lee, A. Nazzel, J. E. Vasquez, and R. J. Savoy, Phys. Rev. Lett. **58**, 2482 (1987).
[10]Z. Fisk, J. D. Thompson, E. Zirngiebl, J. L. Smith, and S.-W. Cheong, Solid State Commun. **62**, 743 (1987).
[11]K. N. Yang, Y. Dalichaouch, J. M. Ferreira, B. W. Lee, J. J. Neumeier, M. S. Torikachvili, H. Zhou, M. B. Maple, and R. R. Hake, Solid State Commun. **63**, 515 (1987).
[12]G. van der Laan, C. Westra, C. Haas, and G. A. Sawatzky, Phys. Rev. B **23**, 4369 (1981).
[13]G. van der Laan, Solid State Commun. **42**, 165 (1982).
[14]G. A. Sawatzky, in *Studies in Inorganic Chemistry,* edited by R. Metselaar, H. J. M. Heijligers, and J. Schoonman (Elsevier, Amsterdam, 1983), Vol. 3, p. 3.
[15]A. Fujimori and F. Minami, Phys. Rev. B **30**, 957 (1984).
[16]G. A. Sawatzky and J. W. Allen, Phys. Rev. Lett. **53**, 2339 (1985).
[17]J. W. Allen, J. Magn. Magn. Mater. **47-48**, 168 (1985).
[18]J. Zaanen, G. A. Sawatzky, and J. W. Allen, Phys. Rev. Lett. **55**, 418 (1985).
[19]G. van der Laan, J. Zaanen, and G. A. Sawatzky, Phys. Rev. B **33**, 4253 (1986).
[20]J. Zaanen, C. Westra, and G. A. Sawatzky, Phys. Rev. B **33**, 8060 (1986).
[21]L. Ley, M. Taniguchi, J. Ghijsen, R. L. Johnson, and A. Fujimori, Phys. Rev. B **35**, 2839 (1987).
[22]A. Fujimori, M. Saeki, N. Kimizuka, M. Taniguchi, and S. Suga, Phys. Rev. B **34**, 7318 (1987).
[23]P. W. Anderson, Science **235**, 1196 (1987).
[24]G. Baskaran, Z. Sou, and P. W. Anderson, Solid State Commun. **63**, 973 (1987).
[25]P. W. Anderson, G. Baskaran, Z. Zou, and T. Hsu, Phys. Rev. Lett. **58**, 2790 (1987).
[26]H. B. Schüttler, M. Jarrell, and D. J. Scalapino, Solid State Commun. (to be published).
[27]C. M. Varma, S. Schmitt-Rink, and E. Abrahams, Solid State Commun. **62**, 681 (1987).
[28]S. Robaszkiewicz, R. Micnas, and J. Ranninger, Phys. Rev. B **36**, 180 (1987).
[29]H. Aoki and H. Kamimura, Solid State Commun. (to be published).
[30]V. J. Emery, Phys. Rev. Lett. **58**, 2794 (1987).
[31]J. E. Hirsch, Phys. Rev. B **35**, 8726 (1987).
[32]D. H. Lee and J. Ihm, Solid State Commun. **62**, 811 (1987).
[33]A. Fujimori, E. Takayama-Muromachi, Y. Uchida, and B. Okai, Phys. Rev. B **35**, 8814 (1987).
[34]J. A. Yarmoff, D. R. Clarke, W. Drube, U. O. Karlsson, A. Taleb-Ibraham, and F. J. Himpsel, Phys. Rev. B **36**, 3967 (1987).
[35]M. Onellion, Y. Chang, D. W. Niles, R. Joynt, G. Margaritondo, N. G. Stoffel, and J. M. Tarascon, Phys. Rev. B **36**, 819 (1987).
[36]P. Thiry, G. Rossi, Y. Petroff, A. Revcolevschi, and J. Jegoudez, Phys. Rev. B (to be published).
[37]P. D. Johnson, S. L. Qiu, L. Jiang, M. W. Ruckman, Myron Strongin, S. L. Hurlbert, R. F. Garrett, B. Sinkovic, N. V. Smith, R. J. Cava, C. S. Jee, N. Nichols, E. Kaczanowicz, R. E. Salomon, and J. E. Crow, Phys. Rev. B **35**, 8811 (1987).
[38]S.-J. Oh, J. W. Allen, I. Lindau, and J. C. Mikkelsen, Jr., Phys. Rev. B **26**, 4845 (1982).
[39]M. R. Thüler, R. L. Benbow, and Z. Hurych, Phys. Rev. B **26**, 669 (1982).
[40]B. Reihl, T. Riesterer, J. G. Bednorz, and K. A. Müller, Phys. Rev. B **35**, 8804 (1987).
[41]R. L. Kurtz, R. C. Stockbauer, D. Mueller, A. Shih, L. E. Toth, M. Osofsky, and S. E. Wolf, Phys. Rev. B **36**, 8818 (1986).
[42]S. Horn, J. Cai, S. A. Shaheen, Y. Jeon, M. Croft, C. L. Chang, and M. L. deBeor, Phys. Rev. B **36**, 3895 (1987).
[43]J. Orenstein, G. A. Thomas, D. H. Rapkine, C. G. Bethea, B. F. Levine, R. J. Cava, E. A. Rietman, and D. W. Johnson, Jr. (unpublished).
[44]L. F. Mattheiss, Phys. Rev. Lett. **58**, 1024 (1987).
[45]L. F. Mattheiss and D. R. Hamann, Solid State Commun. **63**, 395 (1987).
[46]J. J. Yeh and I. Lindau, At. Data and Nucl. Tables **32**, 1 (1985).
[47]D. R. Penn, Phys. Rev. Lett. **42**, 921 (1979).
[48]L. C. Davis, J. Appl. Phys. **59**, R25 (1986).
[49]The Cu $2p$ XPS spectrum of $NaCuO_2$ is very similar to that for CuO and other copper oxides. See J.-S. Kang (unpublished).
[50]J. W. Allen, S.-J. Oh, O. Gunnarsson, K. Schönhammer, M. B. Maple, M. S. Torikachvili, and I. Lindau, Adv. in Phys. **35**, 275 (1986).
[51]L. C. Davis, Phys. Rev. B **25**, 2912 (1982).
[52]U. Fano, Phys. Rev. **124**, 1866 (1961).
[53]Jun-ichi Igarashi and T. Nakano, J. Phys. Soc. Jpn. (to be published).
[54]M. Aono, T.-C. Chiang, F. J. Himpsel, and D. E. Eastman, Solid State Commun. **37**, 471 (1981).
[55]J. Sugar, Phys. Rev. B **5**, 1785 (1972).
[56]O. Gunnarsson and K. Schönhammer, in *Giant Resonances in Atoms, Molecules and Solids,* edited by J. P. Connerade, J.-M. Esteve, and R. C. Karnatak, Proceedings of NATO Summer School, Les Houches, June 1986 (Plenum, New York, 1987), p. 405.
[57]O. Gunnarson and T. C. Li, Phys. Rev. B (to be published).
[58]M. H. Hecht and I. Lindau, Phys. Rev. Lett. **47**, 821 (1981).
[59]T. B. Lucatorto, T. J. McIlrth, J. Sugar, and S. M. Younger, Phys. Rev. Lett. **47**, 1124 (1981).
[60]J. P. Connerade and M. W. D. Mansfield, Phys. Rev. Lett. **48**, 131 (1982).
[61]A. Rosencwaig and G. K. Wertheim, J. Electron Spectrosc. Relat. Phenom. **1**, 493 (1972).
[62]W. Geertsma, thesis, University of Groningen, 1979 (unpublished).
[63]J. Zaanen and G. A. Sawatzky, Can. J. Phys. (to be published).
[64]P. W. Anderson, Phys. Rev. **115**, 2 (1959).
[65]J. B. Goodenough, *Magnetism and the Chemical Bond* (Wiley, New York, 1963), Table VIII.
[66]G. A. Sawatzky (private communication) has pointed out the possibility that for the large T values here, a bound state with small spectral weight can be pushed out of the continuum and that there can be a series of these if the multiplet splitting of the d^8 state is included. With broadening, such a series could produce a region of low spectral weight near E_F, as observed.
[67]A. Fujimori, E. Takayama-Muromachi, and Y. Uchida, Solid State Commun. (to be published).
[68]R. M. Martin and J. W. Allen, J. Appl. Phys. **50**, 7561 (1979).